



Article

Antibacterial and Photocatalytic Activities of LDH-Based Sorbents of Different Compositions

Anna Maria Cardinale ^{1,*}, Stefano Alberti ¹, Andrea Pietro Reverberi ¹, Michelina Catauro ², Nicolò Ghibaudo ¹ and Marco Fortunato ¹

¹ DCCI, Department of Chemistry and Industrial Chemistry, Università degli Studi di Genova, Via Dodecaneso 31, 16146 Genova, Italy; stefano.alberti@unige.it (S.A.); andrea.reverberi@unige.it (A.P.R.); nicolo.ghibaudo@edu.unige.it (N.G.)

² Department of Engineering, University of Campania “Luigi Vanvitelli”, Via Roma 29, 81031 Aversa, Italy; michelina.catauro@unicampania.it

* Correspondence: cardinal@chimica.unige.it; Tel.: +39-010-3536156

Abstract: Layered double hydroxides (LDHs) play a fundamental role in the processes for the abatement of pollutants in water, with reference to heavy metal decontamination. The research on the topic is multiobjective target oriented, aiming at combining environmental remediation with the possibility of reusing a sorbent as many times as possible, turning it into a renewable resource. In this study, the antibacterial and catalytic properties of a ZnAl-SO₄ LDH and its resulting product after being subjected to a Cr(VI) remediation process are compared. Both solid substrates have also been tested after undergoing a thermal annealing process. The sorbent (previously described and tested for remediation) has been investigated for its antibacterial activity in view of further surgery and drug delivery applications. Finally, its photocatalytic properties have been experimentally tested in the degradation of a model pollutant, i.e., Methyl Orange (MO), under solar-simulated light. Identifying the best recycling strategy for these materials requires an accurate knowledge of their physicochemical properties. The results show that both the antimicrobial activity and the photocatalytic performance may considerably improve after thermal annealing.

Keywords: ZnAl LDH; chromium (VI) removal; heterogeneous photocatalysis; water remediation; pollutants degradation; antimicrobial behaviour



Citation: Cardinale, A.M.; Alberti, S.; Reverberi, A.P.; Catauro, M.; Ghibaudo, N.; Fortunato, M.

Antibacterial and Photocatalytic Activities of LDH-Based Sorbents of Different Compositions.

Microorganisms **2023**, *11*, 1045.

<https://doi.org/10.3390/microorganisms11041045>

Academic Editor: Takashi Onodera

Received: 24 March 2023

Revised: 13 April 2023

Accepted: 14 April 2023

Published: 16 April 2023



Copyright: © 2023 by the authors. Licensee MDPI, Basel, Switzerland. This article is an open access article distributed under the terms and conditions of the Creative Commons Attribution (CC BY) license (<https://creativecommons.org/licenses/by/4.0/>).

1. Introduction

Layered double hydroxides (LDHs) represent a wide ensemble of compounds currently in the hotspot of scientific research owing to their extreme versatility in many applications. From a compositional point of view, they are hydroxides of divalent and trivalent cations of general expression $[M(II)_{1-x}M(III)_x(OH)_2]^{x+}[(A^{n-})_{x/n}mH_2O]$, and they are characterized by a double positively charged brucite-layer, separated by a negatively charged interlayer where host anions are present and replaceable, thus making them useful as anionic exchangers generally known as “anionic clays”.

Initially used as materials with excellent sorption properties, they proved to be particularly suitable in the adsorption of both anions [1] and cations, with obviously different physicochemical mechanisms according to the charge of the species to be retained. In the first case, the M(II)/M(III) molar ratio was one of the most important parameters tuning the anion affinity [2], which has been widely tested in experimental studies concerning halogenated anions of type X^- ($X = F, Cl, Br, I$), related oxoanions such as XO_3^- ($X = Cl, Br, I$) and other specific anions having well-established toxic properties towards the environment and even carcinogenic activity for mammals [3–5], as thoroughly reviewed by [6].

The sorption efficiency of LDHs towards inorganic cations [7] was amply tested in environmental remediation thanks to their selective affinity for polluting species such as Pb(II), Hg(II), Cd(II) and even radioactive isotopes as by-products deriving from nuclear

power plants producing liquid radioactive wastes [8]. In this context, the review paper by [9] is a very exhaustive survey, giving a very wide picture of LDHs of different compositions as adsorbing substrates. They analyzed the mechanisms of heavy metals capture, where chemical precipitation [10], cation complexation and electrostatic attraction [11] at the LDH surface are the most important phenomena governing the abatement of such noxious species. In many cases of heavy metal decontamination, LDH adsorption performances proved to be competitive, in both economic and management terms, with those offered by the corresponding biosorption processes [12].

In addition to their affinity to both cations and anions, LDHs as sorbents also have a very interesting peculiarity: they proved to be likewise efficient in the abatement of organic polluting compounds, including dyes, pesticides [13] and pharmaceuticals [14], the latter representing a crucial subset of emerging contaminants affecting developing countries, where a high concentration of antibiotics have been detected in soils and water [15]. In the comprehensive survey presented by [16] about correlations between the structure and sorption efficiency of LDHs, authors pointed out that the main processes governing the adsorption of organic pollutants are based on outer surface sorption and interlayer anion exchange, having a basic role in the presence of anionic molecules like Methyl Orange (MO), which can be assumed as a sort of prototypical dye in the current literature on the topic. Interestingly, they stressed that there is still a lack of investigation concerning the role of interlayer orientation in determining the LDHs' sorption performances, which can be dramatically low in the presence of organic molecules with a predominance of cationic groups [17].

The versatility of LDH use is proven by their results as efficient catalysts and photocatalysts with a broad spectrum of structural and compositional variants [18]. In the first case, the LDH served as a substrate for host molecules already employed as homogeneous catalysts. With such a strategy, the drawbacks typical of homogeneous catalysis can be overcome, with benefits in terms of thermal stability and product separation [19]. On that note, the production of valuable chemicals by CO₂ conversion [20], such as CO₂ hydrogenation to methanol and hydrocarbons, by LDH-based catalysts are well-known and challenging fields of research, in line with the recent protocols of green energy and sustainable manufacturing, where the minimization of greenhouse gases is a pressing target [21]. In this context, against a large amount of experimental data, there is a growing and pressing need for accurate modeling of reaction kinetics, which does not seem to have been developed with the same trend, as pointed out by some investigators, also considering that the best opportunities for a safer process development are connected to the early-stage development [22]. In the second case, the more recent findings in LDH-driven photocatalysis have ushered a new phase in LDH research and applications, as the possibility of compositional and structural variants in the choice of LDH photocatalysts is even greater than the one typical of the conventional LDH-based catalysts [23]. In the line of research focused on LDH-assisted photocatalysis, two trends can be distinguished. The first one is focused on pristine LDH materials, which can be considered as homogeneous photocatalysts whose efficiency can be tuned by varying both cation composition and M(II)/M(III) ratio in the brucite layers, as adopted in CO₂ photoreduction of the first generation [24,25]. However, the efficiency of genuine LDH photocatalysts suffers from some serious drawbacks related both to a limited specific surface area and to an intrinsically small diffusivity of charge carriers to the surface, thus acting as rate-limiting steps dramatically affecting the overall kinetics of photocatalytic reactions. The advent of surface nanotechnology allowed these disadvantages to be overcome by new synthesis techniques to produce monolayered or ultrathin-layered LDH photocatalysts with promising results in artificial photosynthesis [26], nitrogen oxide conversion to nitrate ion [27] and NH₃ synthesis by N₂ photoreduction [28]. The second trend concerns the realization of composite and hybrid photocatalysts, where an LDH-based structure is coupled with different co-catalysts, whose heterojunction has a basic role in reducing electron-hole recombination with a significant increase in chemical process yield, independently of the specific reaction [29]. Likewise,

the negative effect of a large bandgap, making the use of UV light almost mandatory, can now be considerably damped, thus making composite LDH photocatalysts useful in water splitting by visible light [30]. These hybrid and composite LDH-based mixtures allowed the realization of sensors for trace-level analysis of organic and inorganic pollutants [31], with important applications in many fields of analytical chemistry [32], including optical sensing [33].

The recent use of LDHs as antibacterial substrates is further recent proof of LDH versatility in their multipurpose applications [34,35]. For example, Ref. [36] synthesized LDH-organic composites by intercalation of benzoic acid derivatives between Zn-Al LDH interlayers using an anionic exchange technique. The antibacterial properties of the as-prepared composite were tested against colonies of Gram-positive and negative pathogens.

The present study can be traced back to this context in that a ZnAl-SO₄ LDH substrate has been tested for photocatalytic and antibacterial properties in four different structural and compositional variants. The novel aspects of this study consist of applying the three Rs (Reduce, Reuse, Recycle) philosophy to an eco-friendly compound primarily useful in the remediation field. The paper is divided as follows. In Section 2, the synthesis process is described, together with the characterization techniques. In Section 3, the results are presented both for the photocatalytic activity with respect to the abatement of a selected benchmark target molecule and for the antibacterial activity against standard pathogens. In Section 4, the conclusions are drawn, and a future research line is traced.

2. Materials and Methods

2.1. Reagents for Synthesis, Photocatalytic and Antimicrobial Tests

Aluminum sulfate (Al₂(SO₄)₃·9H₂O, 99%, VWR Chemicals, Leuven, Belgium), zinc nitrate (Zn(NO₃)₂·7H₂O, 99%, VWR Chemicals, Leuven, Belgium), sodium hydroxide (NaOH, >97%, Merck, Milano, Italy), potassium chromate (K₂CrO₄, >99%, Sigma Aldrich, St. Louis, MO, USA), Methyl Orange (MO, C₁₄H₁₄N₃NaO₃S, >98%, Merck, Darmstadt, Germany) were used as purchased. For chromium binding experiments, the latter reagent was used to prepare calibrated solutions of 1000 mg/L K₂CrO₄ in water. All reactions were carried out in aqueous solvent, using deionized water produced by an ionic exchange unit (M3/M6 Chemical Bürger s.a.s, Genova, Italy).

The assessment of antimicrobial activity was carried out using *Escherichia coli* strains (ATCC25922), *Staphylococcus aureus* strains (ATCC25923), TBX Medium (Tryptone Bile X-Gluc), Baird Parker Agar Base, Egg Yolk Tellurite emulsion 20% and isotonic sodium chloride solution (NaCl, 0.9% in water). All reagents for antimicrobial tests were purchased from Liofilchem S.r.l., Teramo, Italy.

2.2. LDH Synthesis

The synthesis of the ZnAl sulfate-LDH, with a molar ratio Zn/Al = 3, has been carried out following a standard procedure [7], relying upon a coprecipitation reaction followed by an aging process under heating. In all experiments, the deionized water used in each synthesis step was decarbonated by boiling and further stripping by argon to minimize the presence of CO₂ in the reaction environment. For the same reason, the global process was carried out under argon atmosphere to avoid contamination by CO₃²⁻ anions in the interlayer structure, where only SO₄²⁻ anions should be present, to maximize the overall LDH performances.

The two sulfates, previously weighted and mixed according to the Zn/Al molar ratio, were dissolved in 150 mL of boiled deionized water and kept at rest in a beaker under argon atmosphere. A three-necked flask, where 200 mL of deionized water was put and kept in agitation by a magnetic stirrer, served as a reactor equipped by an electrode for pH measurement. The pH value was monitored by means of a pH-meter pH/ORP/ISE Single Channel Benchtop Meter-HI3221 (HANNA Instruments, Woonsocket, RI, USA).

Afterward, the aqueous phase carrying the mixed sulfates was added dropwise into the flask, keeping the pH constantly fixed at 8 ± 0.5 by continuously adding NaOH solution

dropwise. Sodium hydroxide not only acted as a reagent, but it allowed an online correction of the holdup pH. For this reason, it was separately prepared in solutions having growing concentrations up to 2 M to ensure a timely intervention if required. The whole process was carried out under magnetic stirring at approximately 900 r.p.m.

Once the mixing of the reagents was complete, the solution embedding the as-formed solid phase was transferred into a dark sealed vessel, and the suspension was aged in a stove at 50 °C for a week. This relatively long-standing time was necessary so that the solid could attain a stable crystalline structure. Afterward, the as-formed crystalline LDH was separated by filtration, repeatedly washed with water and finally dried in a static oven at 50 °C for 24 h. The yield of the processes is about 80%.

The product obtained according to this synthesis procedure underwent different and mutually exclusive after-synthesis processes. From this point on, for the sake of clarity, the three different solid phases tested in the remainder of this study will be named ZnAl-SO₄ LDH, ZnAl-MMO (mixed metals oxide), ZnAl-CrO₄ LDH and ZnAl-MMO-CrO₄ according to the following scheme:

- ZnAl-SO₄ LDH is the pristine LDH phase, with no after-synthesis process.
- ZnAl-MMO is the phase obtained by the ZnAl-SO₄ LDH annealing at 450 °C for 5 h. This process transforms the pristine LDH structure in ZnAl mixed oxide, whose structure maintains a certain disorder degree.
- ZnAl-CrO₄ LDH is the phase resulting from Cr(VI) adsorption, up to saturation, on a pristine ZnAl-SO₄ LDH sorbent, according to a protocol described in a previous study [37].
- ZnAl-MMO-CrO₄ is the mixed oxide from the annealing process saturated with Cr(VI).

2.3. Characterization Techniques

All the compounds, after being prepared, were characterized by means of several techniques: Inductively Coupled Plasma-Atomic Emission Spectroscopy (ICP-AES), X-ray powder diffraction (XRPD), Field Emission Scanning Electron Microscope (FE-SEM) and Fourier Transform Infrared Spectroscopy (FT-IR). The ICP-AES measurements were performed using an axially-viewed Varian (Springvale, Australia) Vista PRO. The sample introduction system consisted of a glass concentric K-style pneumatic nebulizer (Varian) jointed to a glass cyclonic spray chamber (Varian). To compensate for non-spectral interferences, the online internal standardization (4 µg mL⁻¹ Lu standard solution) was applied. XRPD patterns were collected to identify the eventual crystalline phase using X'Pert MPD (Philips, Almelo, Netherland) X-ray powder diffractometers equipped with a Cu anticathode with Cu Kα1 radiation ($\lambda = 1.5406 \text{ \AA}$), the samples were prepared by grinding them in an agate mortar. The patterns were collected between 10° and 100° 2θ with a step of 0.001° and measuring time of 50 s/step.

The indexing of the obtained diffraction data was performed by comparison of signals with those available in the literature [37], and the lattice parameters of the phases were calculated using the LATCON program [38]. A ZEISS SUPRA 40 V model of the field emission scanning electron microscope (FE-SEM) was used, where the sample was analyzed by applying an acceleration voltage of 5 kV for 50 s. FT-IR spectra were collected in the usual wavelength range from 4000 to 600 cm⁻¹ using a Spectrum 65 FT-IR Spectrometer (PerkinElmer, Waltham, MA, USA) equipped with a KBr beam-splitter and a DTGS detector by using an ATR accessory with a diamond crystal.

2.4. Antimicrobial Activity Tests

The following procedure has been applied to evaluate the antimicrobial activity of ZnAl-SO₄ LDH and ZnAl-MMO. The bacteria used for this test were both Gram-negative (*Escherichia coli*) and Gram-positive (*Staphylococcus aureus*) incubated in the presence and absence of the sample.

Prior to the analysis, the sample powder was compressed into two small disks of 150 mg and 300 mg, respectively. These disks were then sterilized under UV light for 1 h.

TBX Medium (Tryptone Bile X-Gluc) and Baird Parker Agar Base were prepared by dissolving each nutrient in autoclaved water. Each bacterial media was sterilized at 120 °C for 15 min and slowly cooled. TBX was poured directly into Petri dishes at 50 °C, while the Baird Parker Agar was cooled up to 50 °C and enriched with Egg Yolk Tellurite emulsion 20%.

The antimicrobial properties were evaluated using the Kirby–Bauer method [39,40]. The pellets of the bacterial strains were dissolved in isotonic saline water (0.9% NaCl) and diluted, obtaining bacterial suspensions of 105 CFU/mL, which were plated on the respective solid agar media. *E. coli* was plated on TBX Medium and *S. aureus* on Baird Parker Agar. Before the incubation time of bacteria, the sample disks of 150 and 300 mg were placed in the middle of Petri dishes. *E. coli* was incubated at 44 °C for 24 h, while *S. aureus* was incubated at 36 °C for 24 h. To evaluate the antimicrobial activity, after the incubation time, the diameters of the inhibition halos (IHDs) were calculated. For each sample, to determine the mean Standard Deviation, four measures of the diameter were taken.

2.5. Photocatalytic Experiments Setup

Photocatalytic experiments were performed to investigate the possibility of reusing the tested ZnAl-SO₄ LDH materials, before and after the Cr(VI) remediation process as well as before and after a thermal treatment, for environmental purposes. Since the capability of some layered double hydroxide materials to act as heterogeneous photocatalysts are reported in the literature, it was decided to test the photocatalytic performances of the substrates listed at the end of Section 2.2 (Table 1) for water purification from emerging contaminants [41–44].

Table 1. Scheme of the substrates used in the present tests concerning photocatalytic abatement of contaminants.

Sample n.	Composition
1	ZnAl-SO ₄ LDH
2	ZnAl-MMO
3	ZnAl-CrO ₄ LDH
4	ZnAl-MMO-CrO ₄

A volume of 50 mL of 0.01 g L⁻¹ (10 ppm) Methyl Orange (MO) aqueous solution (pH = 5.5, T = 293 K) was employed as a model pollutant: powdered samples were dispersed within the solution at a concentration equal to 0.25 mg mL⁻¹ and subjected to solar simulated light irradiation with an OSRAM Ultra-Vitalux lamp (300 W) placed 20 cm above the solutions. MO dye, being a typically recalcitrant pollutant, was chosen as a test molecule for assessing photocatalysts' activity. Solar lamp's irradiance is reported to be 1.1 W m⁻² in the UV-B range, 7.3 W m⁻² in the UV-A range and 29.7 W m⁻² in the Vis range. Experiments were performed for a total of 120 min while aliquots were withdrawn every 15 min. The percentage degradation Deg (%) of the dye was measured according to the following equation:

$$\text{Deg (\%)} = (C_0 - C_t) / C_0 \times 100 \quad (1)$$

A blank experiment was performed to study the stability of MO under irradiation, in the same conditions exploited for the photocatalytic tests but without the dispersed material. Further, to investigate the adsorption/desorption equilibrium between tested materials and MO, thus the contribution of the photocatalytic process, the same experiments were performed in dark conditions, without lamp irradiation. Adsorption kinetics were investigated for tested samples by modeling both pseudo-first-order and pseudo-second-order, according to [45–48]. Prior to the analysis, aliquots withdrawn from the solution were subjected to 13,200 rpm centrifugation for 10 min to remove suspended materials,

and eventually, MO concentration was quantified using a UV-Vis LAMBDA 35 (Perkin Elmer, Waltham, MA, USA) spectrophotometer, monitoring MO maximum absorbance ($\lambda = 463$ nm). Each sample was tested in duplicate.

3. Results and Discussion

The pristine LDH compound has been characterized, and the results confirm the structure demonstrated in [7]; nevertheless, the TGA curve is reported to explain the annealing temperature chosen. The thermogravimetric pattern for ZnAl-SO₄ LDH, observable in Figure 1, shows three main mass losses, with a global mass decrease of about 33 mass%. The first thermal effect, at about 100 °C, is due to the humidity, while the second one, occurring in a temperature range of 200–550 °C corresponds to the loss of crystallization water and probably to a release of CO₂ entrapped in the structure (as seen in the FTIR spectrum). The last thermal effect, starting at about 710 °C, is attributable to SO₂ gas evolution.

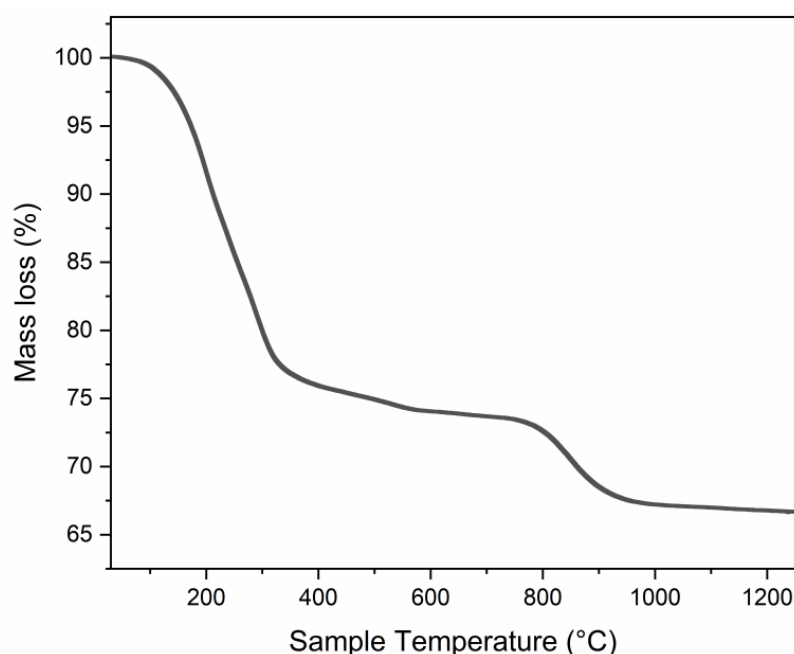


Figure 1. TGA curve for the ZnAl-SO₄ LDH from [7].

Owing to the thermal behavior on heating and according to the literature [49–51], the pristine LDH has been annealed at 450 °C for 5 h to obtain the ZnAl-MMO. In Figure 2, the PXRD patterns for both pristine LDH and ZnAl-MMO resulting from annealing are reported, together with the main reflection indexes. The structure of the mixed oxide, belonging to the space group 186, hP4-ZnO type, can be identified in the ZnAl-MMO.

By comparing the two PXRD patterns, it is highlighted a change in the structure and a transformation of the layered double hydroxide in a Zn Al mixed oxide, which retains a turbostratic structure, as shown by the asymmetric feature of the peaks.

Morphology and composition of the annealed LDH (ZnAl-MMO) have been investigated by FESEM analysis, and the results are reported in Figure 3.

The ZnAl-MMO compound retains the typical lamellar feature, and the EDXS analysis confirms the Zn/Al ratio also in the mixed oxide.

Both the pristine compound and the annealed one have been tested for their antimicrobial behavior, while the samples containing a high concentration of Cr(VI) anion were not subjected to an analogous test.

Figure 4 shows the results of the antimicrobial analysis, and Figure 4B,C reports the values of the inhibition halos.

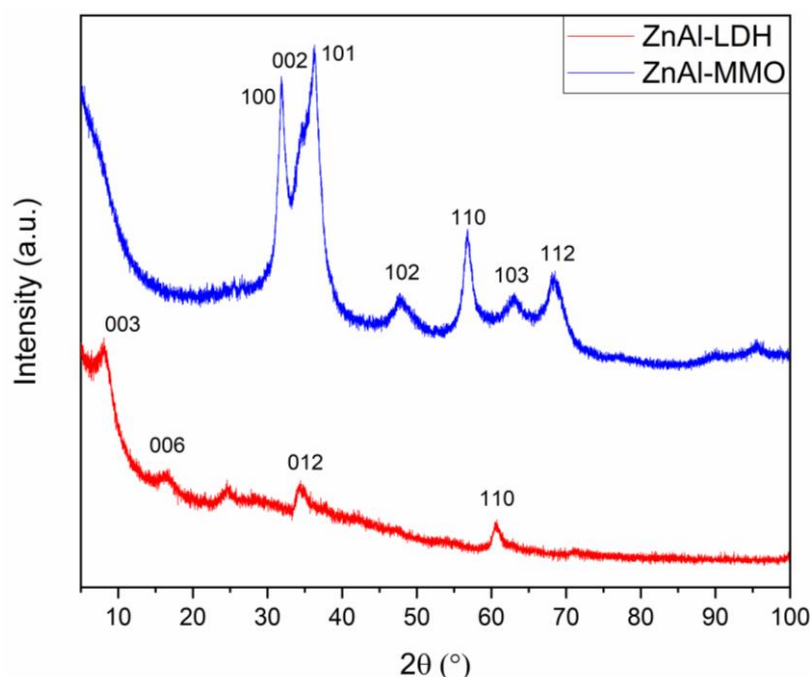


Figure 2. PXRD pattern for the pristine LDH compound (red line) and the ZnAl-MMO (blue line).

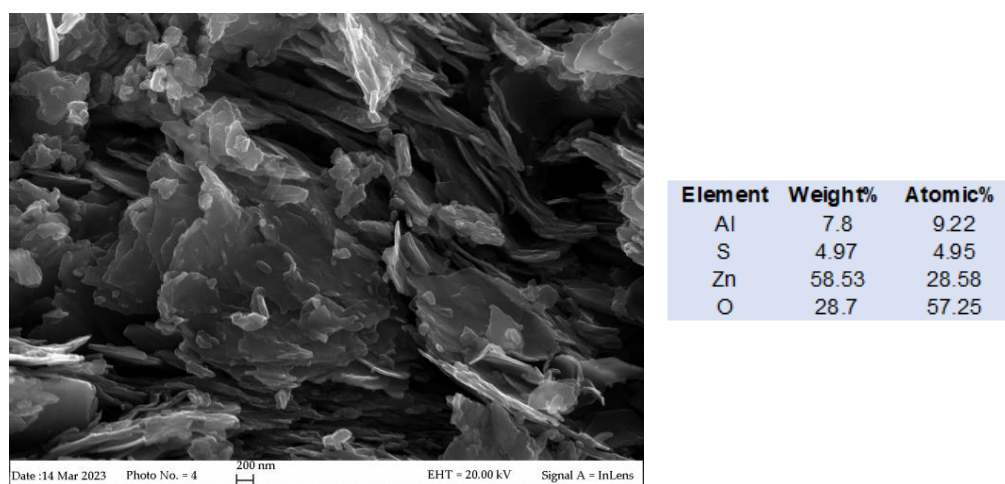


Figure 3. FESEM image of the ZnAl-MMO morphology and composition.

By simple inspection of Figure 4A, the ZnAl-SO₄-LDH, regardless of the amount analyzed, does not have significant antimicrobial activity against both *E. coli* and *S. aureus* bacteria. However, the activity against *E. coli* was slightly higher than the one against *S. aureus*, whose IHDs were equal to the diameters of the sample disks (Figure 4B,C, 1.3 cm), as no growths on them were observed. The average inhibition halos of untreated ZnAl-SO₄-LDH against *E. coli* were 1.95 and 1.79 cm for the 150 and 300 mg disks (Figure 4B,C), respectively. Before thermal treatment, the inhibition power does not seem to be related to the quantity assayed; in fact, the inhibition halo of 150 mg disk is quite equal to the one obtained with 300 mg disk. An explanation could be related to the fact that a larger quantity of material can more easily form complex, leading to the partial loss of the functional groups responsible for the antibacterial activity [52,53]. However, the antimicrobial activity of ZnAl-SO₄ LDH is also reported in the literature [54]. After thermal treatment at 450 °C, the antimicrobial activity seems to be enhanced. Indeed, both bacteria were inhibited by the ZnAl-MMO compound. In particular, the antimicrobial effects against *E. coli* (2.5 and 3.1 cm) were greater than those observed against *S. aureus* (1.8 and 2.3 cm). Moreover, the treatment

also affects the dose-dependent activity. Indeed, an increase in the sample amount resulted in an increase in the IHDs. This is in accordance with the finding that Zn^{2+} , released from ZnO particles interacting with the bacterial media, may have an important antimicrobial activity against *Escherichia coli*, *Staphylococcus aureus*, and *Pseudomonas aeruginosa* [55].

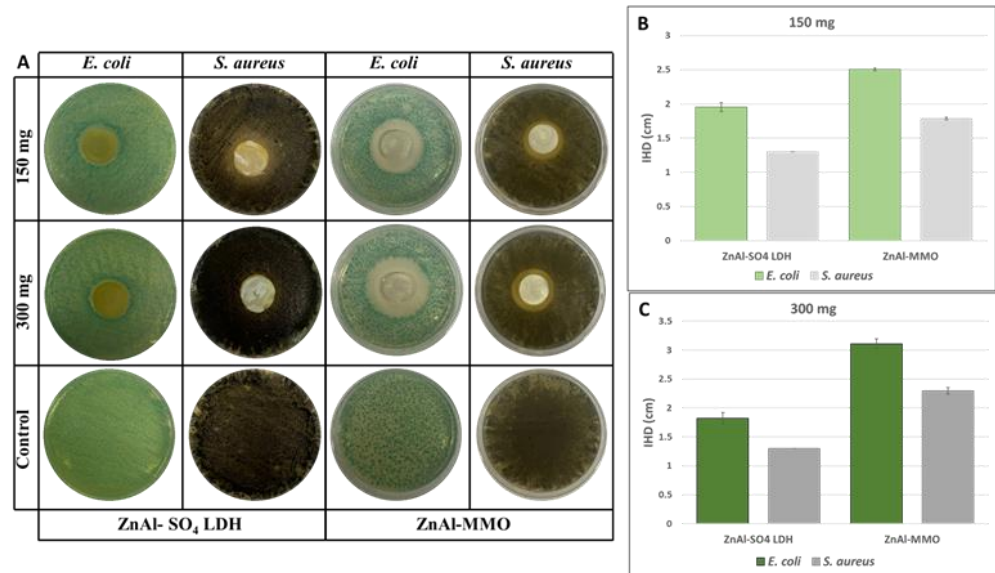


Figure 4. (A) *E. coli* and *S. aureus* images obtained after incubation in the presence and absence of ZnAlSO₄-LDH and ZnAl-MMO. Inhibition halo diameters (IHDs) of ZnAlSO₄-LDH and ZnAl-MMO samples obtained with (B) 150 mg and (C) 300 mg.

The results for the catalytic activity in the dark, thus concerning only adsorption experiments, are reported in Figure 5, while the relevant kinetics, modeled as pseudo-first and pseudo-second-order rate laws, are reported in Table 2.

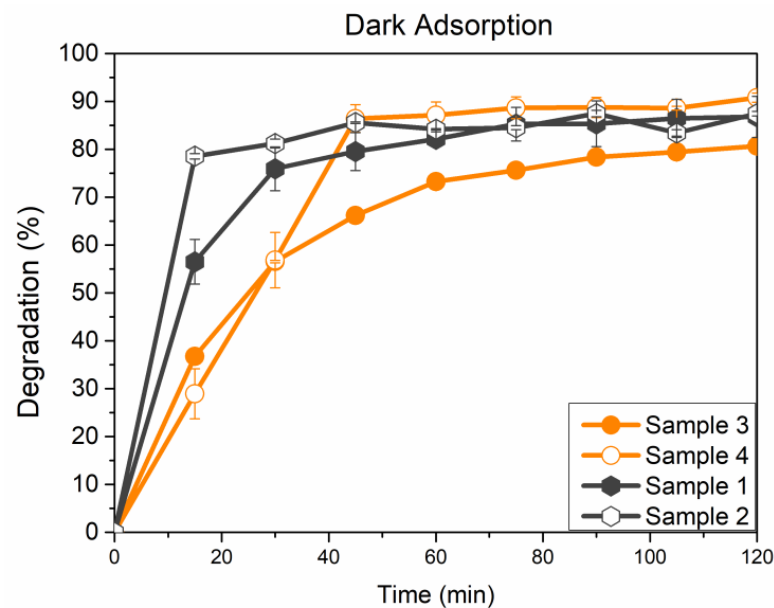


Figure 5. MO percentage degradation (calculated according to Equation (1)) for investigated samples in dark condition.

Table 2. Adsorption kinetic model rate constants for MO on investigated samples.

Sample n.	Pseudo-First-Order eq.	q_e (exp.) (mg g ⁻¹)	q_e (calc.) (mg g ⁻¹)	k_1 (min ⁻¹)	R ²
1	$y = -0.0038x - 1.9017$	0.0378	0.0125	0.0087	0.7974
2	$y = -0.0014x - 2.1001$	0.0373	0.0079	0.0032	0.575
3	$y = -0.0043x - 1.7303$	0.0356	0.0186	0.0099	0.8928
4	$y = -0.0067x - 1.7674$	0.0350	0.0170	0.0154	0.6993
Sample n.	Pseudo-Second-Order eq.	q_e (exp.) (mg g ⁻¹)	q_e (calc.) (mg g ⁻¹)	k_2 (g mg ⁻¹ min ⁻¹)	R ²
1	$y = 30.877x + 58.531$	0.0378	0.0355	16.2886	0.9992
2	$y = 31.732x + 20.434$	0.0373	0.0288	49.2766	0.9985
3	$y = 34.666x + 169.79$	0.0356	0.0315	7.0777	0.9955
4	$y = 28.122x + 104.29$	0.0350	0.0323	7.5831	0.9944

All the experiments performed in dark conditions are reported in Figure 5. All tested materials show a quite pronounced tendency to interact with the MO dye, specifically showing surface adsorption, which subtracts the dye from the solution. Samples show similar behavior and reach an average final value of 85% in MO degradation (%) after 120 min in all cases. Instead, considering the first 15 min, some differences can be observed: Sample 3 and Sample 4 are slower in the MO adsorption, probably because they already absorbed chromate ions within their structure. Sample 1 and Sample 2, at the same time, double the percentage of MO adsorbed with respect to Samples 3 and 4. The calcination process has likely modified the materials' features, as in both cases, a slight increase in the MO adsorbed concentration can be noticed. Finally, all samples attained an adsorption-desorption equilibrium in the first hour of the experiment, ending with a high value of dye adsorption. According to the observed results, the experimental data were better fitted by a pseudo-second-order kinetics rate law, as shown by R² values, which are quite high (>0.99) when compared to pseudo-first-order ones. Furthermore, the values of q_e computed using a pseudo-second-order model are closer to the corresponding experimental values than the ones obtained by adopting a first-order kinetics model.

To try out the heterogeneous photocatalytic performance of the tested materials, the same experiments were performed under simulated solar light exposure, and results are reported in Figure 6b, while Figure 6a reports the results concerning MO stability under irradiation.

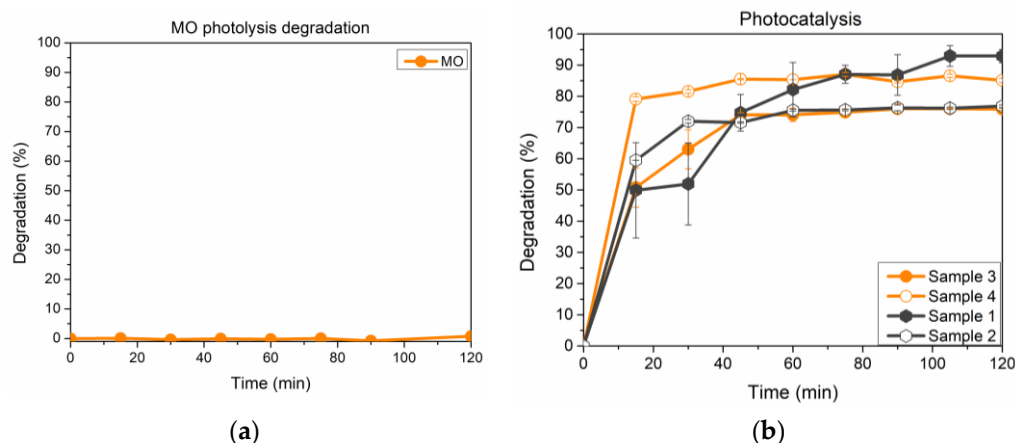


Figure 6. (a) MO percentage degradation due to photolysis (MO stability under irradiation); (b) MO percentage degradation (calculated according to Equation (1)) for investigated samples under solar simulated light.

Methyl Orange itself proved to be stable under solar light exposure, as no change in the concentration was detected. Unfortunately, samples still show a marked tendency to adsorb MO dye in a way that makes it difficult to ascertain the effect of photocatalysis. To clarify this trend, another test run was carried out at the same experimental conditions before irradiation, with samples left under stirring in the dark for 60 min. Namely, Figure 6 shows that all solid substrates interact with MO in the first 60 min, after which the concentration remains stable. The photocatalytic test is then carried out for an additional 60 min, and the results are reported in Figure 7.

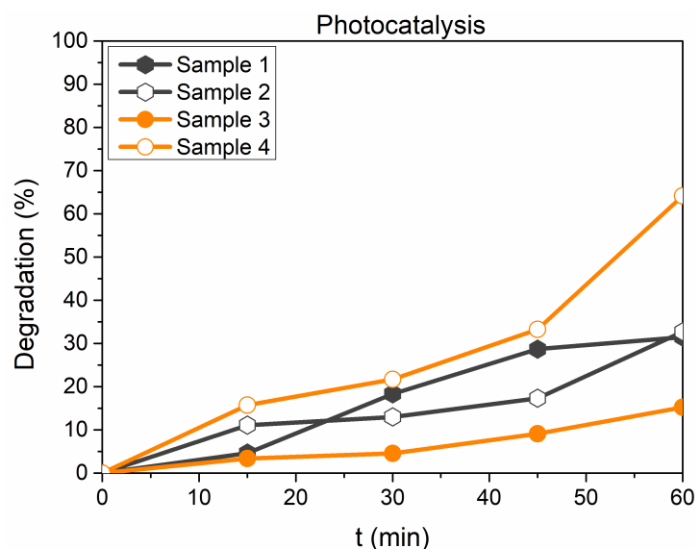


Figure 7. MO percentage degradation (calculated according to Equation (1)) for investigated samples.

As a general conclusion, it seems that Samples 1 and 2 strongly interact with the dye in dark conditions, and this implies that adsorption occurs on the sample's surface; the same interaction can be observed for Samples 3 and 4, even though the rate of adsorption is slower. After an initial adsorption phase, when solar light irradiation is switched on, Sample 4 turns out to be the most performing, as it can reach a final abatement of 60% only due to irradiation. Furthermore, the dye degradation obtained by the same sample without thermal treatment stands at around 15%, proving that the thermal treatment strongly influences the photocatalytic trend. Both samples 1 and 2 achieve a final abatement degree of 30% without any changes relating to the thermal process. This could be reasonably ascribed to the tendency of the material to adsorb chemical species present in the liquid phase: whenever the samples are pre-treated as adsorbers, the photocatalytic activity is predominant over the adsorption process. On the opposite, bare samples have a significant tendency to adsorb the dye instead of degrading it.

4. Conclusions

In the present study, ZnAl-SO₄ LDH substrates and other solid matrices derived from them have been investigated for their photocatalytic and antimicrobial properties. The most important results can be summarized in the following points:

- The antimicrobial activity increases after heat treatment is performed, which moreover influences the effect of dose dependence. This result may open interesting new scenarios in drug delivery field applications.
- The photocatalytic activity of the investigated compounds is well described by pseudo-second-order kinetics, despite the calculated values of q_e , for both pseudo-first- and pseudo-second-order kinetics are not markedly different.
- The overall performances are affected by adsorption phenomena, and this result is more pronounced for the two compounds without the chromate anion. The results seem to suggest that the presence of chromate ions within the structure may influence

the photocatalytic activities of these materials, thus creating new opportunities in recycling exhaust LDH, having adsorbed contaminants like Cr(VI), by turning it into a photocatalyst of promising performances. On the other hand, an increase of catalytic activity following the adsorption of Cr(VI) would hamper the use of this substrate for medical or drug delivery purposes, owing to the well-known toxicity of the adsorbed anion.

Author Contributions: Conceptualization, A.M.C. and M.F.; methodology, all authors; software, all authors.; validation, A.M.C. and A.P.R.; formal analysis, all authors; investigation, A.M.C., M.C., S.A. and N.G.; resources, A.M.C., M.C. and S.A.; data curatorial, Authors equally contributed; writing—original draft preparation, A.M.C., M.C. and S.A.; writing—review and editing, A.P.R. and A.M.C.; visualization, all authors contributed equally; supervision, A.M.C.; project administration, A.M.C.; funding acquisition, not applicable. All authors have read and agreed to the published version of the manuscript.

Funding: This research received no external funding.

Informed Consent Statement: Not applicable.

Data Availability Statement: Not applicable.

Conflicts of Interest: The authors declare no conflict of interest.

References

1. Premathilaka, R.W.; Liyanagedera, N.D. Fluoride in Drinking Water and Nanotechnological Approaches for Eliminating Excess Fluoride. *J. Nanotechnol.* **2019**, *2019*, 2192383. [[CrossRef](#)]
2. Theiss, F.L.; Couperthwaite, S.J.; Ayoko, G.A.; Frost, R.L. A review of the removal of anions and oxyanions of the halogen elements from aqueous solution by layered double hydroxides. *J. Colloid Interface Sci.* **2014**, *417*, 356–368. [[CrossRef](#)] [[PubMed](#)]
3. Tran, H.N.; Nguyen, D.T.; Le, G.T.; Tomul, F.; Lima, E.C.; Woo, S.H.; Sarmah, A.K.; Nguyen, H.Q.; Nguyen, P.T.; Nguyen, D.D.; et al. Adsorption mechanism of hexavalent chromium onto layered double hydroxides-based adsorbents: A systematic in-depth review. *J. Hazard. Mater.* **2019**, *373*, 258–270. [[CrossRef](#)]
4. Dias, A.C.; Fontes, M.P.F. Arsenic (V) removal from water using hydrotalcites as adsorbents: A critical review. *Appl. Clay Sci.* **2020**, *191*, 105615. [[CrossRef](#)]
5. Wang, J.; Zhang, T.; Li, M.; Yang, Y.; Lu, P.; Ning, P.; Wang, Q. Arsenic removal from water/wastewater using layered double hydroxide derived adsorbents, a critical review. *RSC Adv.* **2018**, *8*, 22694–22709. [[CrossRef](#)] [[PubMed](#)]
6. Goh, K.-H.; Lim, T.-T.; Dong, Z. Application of layered double hydroxides for removal of oxyanions: A review. *Water Res.* **2008**, *42*, 1343–1368. [[CrossRef](#)]
7. Cardinale, A.M.; Carbone, C.; Fortunato, M.; Fabiano, B.; Reverberi, A.P. ZnAl-SO₄ Layered Double Hydroxide and Allophane for Cr(VI), Cu(II) and Fe(III) Adsorption in Wastewater: Structure Comparison and Synergistic Effects. *Materials* **2022**, *15*, 6887. [[CrossRef](#)] [[PubMed](#)]
8. Kobylnska, N.G.; Puzyrnaya, L.M.; Pshinko, G.M. Layered Double Hydroxides as Promising Adsorbents for Purification of Radioactive Polluted Water: A Review. *Theor. Exp. Chem.* **2022**, *58*, 221–239. [[CrossRef](#)]
9. Ahmed, M.A.; Mohamed, A.A. A systematic review of layered double hydroxide-based materials for environmental remediation of heavy metals and dye pollutants. *Inorg. Chem. Commun.* **2023**, *148*, 110325. [[CrossRef](#)]
10. Yang, F.; Sun, S.; Chen, X.; Chang, Y.; Zha, F.; Lei, Z. Mg–Al layered double hydroxides modified clay adsorbents for efficient removal of Pb²⁺, Cu²⁺ and Ni²⁺ from water. *Appl. Clay Sci.* **2016**, *123*, 134–140. [[CrossRef](#)]
11. Zhao, D.; Sheng, G.; Hu, J.; Chen, C.; Wang, X. The adsorption of Pb(II) on Mg₂Al layered double hydroxide. *Chem. Eng. J.* **2011**, *171*, 167–174. [[CrossRef](#)]
12. Beolchini, F.; Pagnanelli, F.; Reverberi, A.P.; Vegliò, F. Copper Biosorption onto *Rhizopus oligosporus*: pH-Edge Tests and Related Kinetic and Equilibrium Modeling. *Ind. Eng. Chem. Res.* **2003**, *42*, 4881–4887. [[CrossRef](#)]
13. Mourid, E.H.; Lakraimi, M.; Legrouri, A. Removal and Release of the 2,4,5-Trichlorophenoxyacetic Acid Herbicide from Wastewater by Layered Double Hydroxides. *J. Inorg. Organomet. Polym. Mater.* **2021**, *31*, 2116–2128. [[CrossRef](#)]
14. Santamaría, L.; Vicente, M.; Korili, S.; Gil, A. Progress in the removal of pharmaceutical compounds from aqueous solution using layered double hydroxides as adsorbents: A review. *J. Environ. Chem. Eng.* **2020**, *8*, 104577. [[CrossRef](#)]
15. Yang, Y.; Owino, A.A.; Gao, Y.; Yan, X.; Xu, C.; Wang, J. Occurrence, composition and risk assessment of antibiotics in soils from Kenya, Africa. *Ecotoxicology* **2016**, *25*, 1194–1201. [[CrossRef](#)] [[PubMed](#)]
16. Johnston, A.-L.; Lester, E.; Williams, O.; Gomes, R.L. Understanding Layered Double Hydroxide properties as sorbent materials for removing organic pollutants from environmental waters. *J. Environ. Chem. Eng.* **2021**, *9*, 105197. [[CrossRef](#)]
17. Li, E.; Liao, L.; Lv, G.; Li, Z.; Yang, C.; Lu, Y. The Interactions between Three Typical PPCPs and LDH. *Front. Chem.* **2018**, *6*, 16. [[CrossRef](#)] [[PubMed](#)]

18. Antoniuk-Jurak, K.; Kowalik, P.; Bicki, R.; Michalska, K.; Próchniak, W.; Wiercioch, P. Cu substituted ZnAl₂O₄ ex-LDH catalysts for medium-temperature WGS—effect of Cu/Zn ratio and thermal treatment on catalyst efficiency. *Int. J. Hydrogen Energy* **2019**, *44*, 27390–27400. [[CrossRef](#)]
19. Li, C.; Wei, M.; Evans, D.G.; Duan, X. Layered Double Hydroxide-based Nanomaterials as Highly Efficient Catalysts and Adsorbents. *Small* **2014**, *10*, 4469–4486. [[CrossRef](#)] [[PubMed](#)]
20. Dewangan, N.; Hui, W.M.; Jayaprakash, S.; Bawah, A.-R.; Poerjoto, A.J.; Jie, T.; Jangam, A.; Hidajat, K.; Kawi, S. Recent progress on layered double hydroxide (LDH) derived metal-based catalysts for CO₂ conversion to valuable chemicals. *Catal. Today* **2020**, *356*, 490–513. [[CrossRef](#)]
21. Fang, X.; Chen, C.; Jia, H.; Li, Y.; Liu, J.; Wang, Y.; Song, Y.; Du, T.; Liu, L. Progress in Adsorption-Enhanced Hydrogenation of CO₂ on Layered Double Hydroxide (LDH) Derived Catalysts. *J. Ind. Eng. Chem.* **2021**, *95*, 16–27. [[CrossRef](#)]
22. Bassani, A.; Vianello, C.; Mocellin, P.; Dell'angelo, A.; Spigno, G.; Fabiano, B.; Maschio, G.; Manenti, F. Aprioristic Integration of Process Operations and Risk Analysis: Definition of the Weighted F&EI-Based Concept and Application to AG2S Technology. *Ind. Eng. Chem. Res.* **2023**, *62*, 500–510. [[CrossRef](#)]
23. Mohanty, U.A.; Sahoo, D.P.; Paramanik, L.; Parida, K. A critical review on layered double hydroxide (LDH)-derived functional nanomaterials as potential and sustainable photocatalysts. *Sustain. Energy Fuels* **2023**, *7*, 1145–1186. [[CrossRef](#)]
24. Wang, C.; Xu, J.; Zhou, Z. A Mini-Review on CO₂ Photoreduction by MgAl-LDH Based Materials. *Energies* **2022**, *15*, 8117. [[CrossRef](#)]
25. Bi, Z.-X.; Guo, R.-T.; Hu, X.; Wang, J.; Chen, X.; Pan, W.-G. Research progress on photocatalytic reduction of CO₂ based on LDH materials. *Nanoscale* **2022**, *14*, 3367–3386. [[CrossRef](#)]
26. Wang, R.; Wang, Z.; Wan, S.; Liu, Q.; Ding, J.; Zhong, Q. Facile layer regulation strategy of layered double hydroxide nanosheets for artificial photosynthesis and mechanism insight. *Chem. Eng. J.* **2022**, *434*, 134434. [[CrossRef](#)]
27. Li, H.; Zhu, H.; Shi, Y.; Shang, H.; Zhang, L.; Wang, J. Vacancy-Rich and Porous NiFe-Layered Double Hydroxide Ultrathin Nanosheets for Efficient Photocatalytic NO Oxidation and Storage. *Environ. Sci. Technol.* **2022**, *56*, 1771–1779. [[CrossRef](#)] [[PubMed](#)]
28. Zhao, Y.; Zhao, Y.; Waterhouse, G.I.N.; Zheng, L.; Cao, X.; Teng, F.; Wu, L.-Z.; Tung, C.-H.; O'Hare, D.; Zhang, T. Layered-Double-Hydroxide Nanosheets as Efficient Visible-Light-Driven Photocatalysts for Dinitrogen Fixation. *Adv. Mater.* **2017**, *29*, 1703828. [[CrossRef](#)]
29. Zhang, M.; Lai, C.; Li, B.; Xu, F.; Huang, D.; Liu, S.; Qin, L.; Liu, X.; Yi, H.; Fu, Y.; et al. Insightful understanding of charge carrier transfer in 2D/2D heterojunction photocatalyst: Ni-Co layered double hydroxides deposited on ornamental g-C₃N₄ ultrathin nanosheet with boosted molecular oxygen activation. *Chem. Eng. J.* **2021**, *422*, 130120. [[CrossRef](#)]
30. Vennapoosa, C.S.; Varangane, S.; Abraham, B.M.; Perupogu, V.; Bojja, S.; Pal, U. Controlled photoinduced electron transfer from g-C₃N₄ to CuCdCe-LDH for efficient visible light hydrogen evolution reaction. *Int. J. Hydrogen Energy* **2022**, *47*, 40227–40241. [[CrossRef](#)]
31. Grover, A.; Mohiuddin, I.; Lee, J.; Brown, R.J.; Malik, A.K.; Aulakh, J.S.; Kim, K.-H. Progress in pre-treatment and extraction of organic and inorganic pollutants by layered double hydroxide for trace-level analysis. *Environ. Res.* **2022**, *214*, 114166. [[CrossRef](#)] [[PubMed](#)]
32. Tang, S.; Yao, Y.; Chen, T.; Kong, D.; Shen, W.; Lee, H.K. Recent advances in the application of layered double hydroxides in analytical chemistry: A review. *Anal. Chim. Acta* **2020**, *1103*, 32–48. [[CrossRef](#)]
33. Sohrabi, H.; Khataee, A.; Ghasemzadeh, S.; Majidi, M.R.; Orooji, Y. Layer double hydroxides (LDHs)- based electrochemical and optical sensing assessments for quantification and identification of heavy metals in water and environment samples: A review of status and prospects. *Trends Environ. Anal. Chem.* **2021**, *31*, e00139. [[CrossRef](#)]
34. Rad, T.S.; Khataee, A.; Arefi-Oskoui, S.; Rad, S.S.; Orooji, Y.; Gengec, E.; Kobya, M. Graphene-based ZnCr layered double hydroxide nanocomposites as bactericidal agents with high sonophotocatalytic performances for degradation of rifampicin. *Chemosphere* **2022**, *286*, 131740. [[CrossRef](#)]
35. Arjomandi-Behzad, L.; Alinejad, Z.; Zandragh, M.R.; Golmohamadi, A.; Vojoudi, H. Facile synthesis of hollow spherical g-C₃N₄@LDH/NCQDs ternary nanostructure for multifunctional antibacterial and photodegradation activities. *iScience* **2023**, *26*, 106213. [[CrossRef](#)] [[PubMed](#)]
36. Mishra, G.; Dash, B.; Pandey, S. Effect of molecular dimension on gallery height, release kinetics and antibacterial activity of Zn Al layered double hydroxide (LDH) encapsulated with benzoate and its derivatives. *Appl. Clay Sci.* **2019**, *181*, 105230. [[CrossRef](#)]
37. Kraus, W.; Nolze, G. Powder Cell for Windows. *Powder Diffr.* **1998**, *13*, 256–259.
38. King, G.; Schwarzenbach Latcon, D. Xtal3.7 System. In *The Gnu Xtal System User's Manual*; Hall, S.R., du Boilay, D.J., Olthof-Hazekamp, R., Eds.; University Of Western: Perth, Australia, 2002.
39. Blanco, I.; Latteri, A.; Cicala, G.; D'angelo, A.; Viola, V.; Arconati, V.; Catauro, M. Antibacterial and Chemical Characterization of Silica-Quercetin-PEG Hybrid Materials Synthesized by Sol-Gel Route. *Molecules* **2022**, *27*, 979. [[CrossRef](#)]
40. Catauro, M.; D'angelo, A.; Fiorentino, M.; Gullifa, G.; Risoluti, R.; Cipriotti, S.V. Thermal behavior, morphology and antibacterial properties study of silica/quercetin nanocomposite materials prepared by sol-gel route. *J. Therm. Anal. Calorim.* **2022**, *147*, 5337–5350. [[CrossRef](#)]
41. Alberti, S.; Doderò, A.; Sartori, E.; Vicini, S.; Ferretti, M.; Castellano, M. Composite Water-Borne Polyurethane Nanofibrous Electrospun Membranes with Photocatalytic Properties. *ACS Appl. Polym. Mater.* **2021**, *3*, 6157–6166. [[CrossRef](#)]

42. Martinelli, A.; Alberti, S.; Caratto, V.; Lova, P.; Locardi, F.; Pampararo, G.; Villa, S.; Ferretti, M. Structural studies on copper and nitrogen doped nanosized anatase. *Z. Für Krist. Cryst. Mater.* **2018**, *233*, 867–876. [[CrossRef](#)]
43. Alberti, S.; Basciu, I.; Vocciante, M.; Ferretti, M. Experimental and Physico-Chemical Comparison of ZnO Nanoparticles' Activity for Photocatalytic Applications in Wastewater Treatment. *Catalysts* **2021**, *11*, 678. [[CrossRef](#)]
44. Alberti, S.; Sotiropoulou, M.; Fernández, E.; Solomou, N.; Ferretti, M.; Psillakis, E. UV-254 degradation of nicotine in natural waters and leachates produced from cigarette butts and heat-not-burn tobacco products. *Environ. Res.* **2021**, *194*, 110695. [[CrossRef](#)] [[PubMed](#)]
45. Mansour, A.T.; Alprol, A.E.; Abualnaja, K.M.; El-Beltagi, H.S.; Ramadan, K.M.A.; Ashour, M. The Using of Nanoparticles of Microalgae in Remediation of Toxic Dye from Industrial Wastewater: Kinetic and Isotherm Studies. *Materials* **2022**, *15*, 3922. [[CrossRef](#)]
46. Gowda, S.A.; Goveas, L.C.; Dakshayini, K. Adsorption of methylene blue by silver nanoparticles synthesized from Urena lobata leaf extract: Kinetics and equilibrium analysis. *Mater. Chem. Phys.* **2022**, *288*, 126431. [[CrossRef](#)]
47. Mondal, U.S.; Das, S.; Somu, P.; Paul, S. Silica sand-supported nano zinc oxide-graphene oxide composite induced rapid photocatalytic decolorization of azo dyes under sunlight and improved antimicrobial activity. *Environ. Sci. Pollut. Res.* **2023**, *30*, 17226–17244. [[CrossRef](#)]
48. Ngoc, P.K.; Mac, T.K.; Nguyen, H.T.; Viet, D.T.; Thanh, T.D.; Van Vinh, P.; Phan, B.T.; Duong, A.T.; Das, R. Superior organic dye removal by CoCr2O4 nanoparticles: Adsorption kinetics and isotherm. *J. Sci. Adv. Mater. Devices* **2022**, *7*, 100438. [[CrossRef](#)]
49. Pinthong, P.; Praserttham, P.; Jongsomjit, B. Effect of Calcination Temperature on Mg-Al Layered Double Hydroxides (LDH) as Promising Catalysts in Oxidative Dehydrogenation of Ethanol to Acetaldehyde. *J. Oleo Sci.* **2019**, *68*, 95–102. [[CrossRef](#)] [[PubMed](#)]
50. Hadnadjev-Kostic, M.; Vulic, T.; Zoric, D.; Marinkovic-Neducin, R. The influence of the UV irradiation intensity on photocatalytic activity of ZnAl layered double hydroxides and derived mixed oxides. *Chem. Ind. Chem. Eng. Q.* **2012**, *18*, 295–303. [[CrossRef](#)]
51. Thite, V.D.; Giripunje, S.M. Adsorption and photocatalytic performance of ZnAl layered double hydroxide nanoparticles in removal of methyl orange dye. *Nanotechnol. Environ. Eng.* **2022**, *7*, 57–66. [[CrossRef](#)]
52. Lok, C.-N.; Ho, C.-M.; Chen, R.; He, Q.-Y.; Yu, W.-Y.; Sun, H.; Tam, P.K.-H.; Chiu, J.-F.; Che, C.-M. Silver nanoparticles: Partial oxidation and antibacterial activities. *JBIC J. Biol. Inorg. Chem.* **2007**, *12*, 527–534. [[CrossRef](#)] [[PubMed](#)]
53. Szunerits, S.; Boukherroub, R. Antibacterial activity of graphene-based materials. *J. Mater. Chem. B* **2016**, *4*, 6892–6912. [[CrossRef](#)] [[PubMed](#)]
54. Hanane, Z.; Kaid, M.; Djamila, I.; Ammam, A.; Villemin, D. Preparation, characterization and antibacterial applications of ZnAl-LDH with the diaminododecylphosphonic acid intercalation. *South Asian J. Exp. Biol.* **2021**, *11*, 600–604. [[CrossRef](#)]
55. Pasquet, J.; Chevalier, Y.; Pelletier, J.; Couval, E.; Bouvier, D.; Bolzinger, M.-A. The contribution of zinc ions to the antimicrobial activity of zinc oxide. *Colloids Surf. A Physicochem. Eng. Asp.* **2014**, *457*, 263–274. [[CrossRef](#)]

Disclaimer/Publisher's Note: The statements, opinions and data contained in all publications are solely those of the individual author(s) and contributor(s) and not of MDPI and/or the editor(s). MDPI and/or the editor(s) disclaim responsibility for any injury to people or property resulting from any ideas, methods, instructions or products referred to in the content.